JOURNAL OF CATALYSIS 141, 124–139 (1993)

The Partial Oxidation of Methane to Formaldehyde: Role of Different Crystal Planes of MoO_3

M. R. SMITH[1] AND U. S. OZKAN[2]

Department of Chemical Engineering, The Ohio State University, Columbus, Ohio 43210

Received October 6, 1992; accepted December 15, 1992

Partial oxidation of methane to formaldehyde was studied over MoO_3 samples which exposed different relative amounts of basal (010) and side (100) plane area. Characterization studies included X-ray diffraction, laser Raman spectroscopy, *in situ* laser Raman spectroscopy combined with isotopic labeling, scanning electron microscopy, three-dimensional imaging technique, X-ray photoelectron spectroscopy, BET surface area measurement, and temperature-programmed reduction. These characterization results were used in conjunction with steady-state reaction studies using methane, formaldehyde, CO, and methanol as the feed over molybdenum trioxide samples to investigate the catalytic anisotropy previously observed over these catalysts for other reaction systems. These studies suggested that the Mo=O sites located on the side plane could be promoting the formation of formaldehyde, while the bridging oxygen sites located on the basal planes were more likely to lead to complete oxidation.

INTRODUCTION

The study of the partial oxidation of methane to formaldehyde and methanol has gained attention in the last decade as researchers search for alternates to the energy intensive steam reforming process (*1*). Many catalysts have been examined in this light, and some of this work has been summarized in recent reviews (*2–4*).

As might be expected, metal oxides have been among the most widely studied catalysts used for methane oxidation. Most of these systems have been mixed oxides such as Bi_2O_3–SnO_2 (*5*) and FeNbB–O (*6*).

Molybdenum trioxide has also been studied for activity and selectivity in methane oxidation, usually as a SiO_2-supported catalyst (*7–14*). Both O_2 and N_2O have been used as oxidants. The mechanism over MoO_3-based catalysts is not, however, completely understood. Liu *et al.* (*7*) studied MoO_3/SiO_2 using N_2O as the oxidant. Spectroscopic evidence indicated the reaction was initiated by the formation of O^- ions at the Mo^{VI} sites at the surface. These ions were responsible for H abstraction from CH_4 to form methyl radicals which react rapidly with the surface to form methoxide complexes. These complexes may then decompose to HCHO, or react with water to form CH_3OH.

Barbaux *et al.* (*9*) have investigated the state of the catalyst surface using surface potential measurements to determine the nature of the oxygen species. They found that N_2O gave O^-, but as the temperature increased above 400°C, O^- was transformed to O^{2-}. They also found that, in the case of O_2 oxidant, methane was probably attacked by O^- species, while with N_2O as oxidant, O^{2-} species reacted with methane, the former leading to the formation of CO_x and the latter giving higher selectivities for HCHO.

The MoO_3/SiO_2 system was also studied by Spencer *et al.* (*10–12*) using O_2 as the oxidant. Kinetic studies showed the reaction pathway to be such that CH_4 is directly

[1] Present address: International Paper, Mobile, Alabama 36652.

[2] To whom correspondence should be addressed.

0021-9517/93 $5.00

oxidized to CO_2 and HCHO, and in turn HCHO is further oxidized to CO, which was the dominant product at higher conversions. Trace amounts of CH_3OH indicated the possibility that it is an intermediate in HCHO formation.

Smith and Ozkan have also examined the partial oxidation of methane to formaldehyde over MoO_3/SiO_2 (*13*). They investigated the surface species formed on the support and their effect on reactivity and selectivity. They found that at low weight loadings, the predominant species was a silicomolybdic species with terminal Mo=O sites. At higher weight loadings, polymolybdate species with Mo–O–Mo bridges began to form at the expense of Mo=O sites. The silicomolybdic species with terminal Mo=O sites were found to have better selectivity for HCHO than the polymolybdate species with Mo–O–Mo bridging sites.

An interesting aspect of MoO_3 is that it has been shown to exhibit structural specificity, a phenomenon which is also referred as catalytic anisotropy in the literature, in selective oxidation reactions (*15–24*). Most of these studies have examined the relationship between the different crystal planes of MoO_3 and their contribution to the activity and selectivity of catalytic reactions. Such studies of catalyst structure are important, as they provide information as to the identification of active sites in these catalysts, as well as clues as to the location of these sites. Volta *et al.* (*15*) prepared MoO_3 crystals which were preferentially oriented on graphite supports. When these catalysts were used for the oxidation of propylene, a correlation between growth of specific MoO_3 crystal planes and an increase in selectivity for acrolein was shown. Similar experiments performed for methanol oxidation (*16*) showed that the (020) faces of MoO_3 were selective for formaldehyde formation. This same group has also investigated unsupported MoO_3 crystals that were preferentially oriented (*17–20*). By combining reaction studies with characterization studies, they postulated that the (120) face is more selective to partial oxidation products due to the stepped atomic structure that is present on this face, bringing the (100) and (010) sites into close proximity. They found the (010) basal planes to be active in total oxidation.

Bruckman *et al.* (*21*) have also investigated the role of different MoO_3 crystal faces in the oxidation of propene. Using allyl compounds to represent intermediates in the reaction pathway, they found that the yield of acrolein from allyl compounds is linearly dependent on the surface area of the basal (010) face, indicating that this face is responsible for insertion of oxygen into the activated hydrocarbon molecule.

The oxidation of C-4 hydrocarbons has also been investigated over MoO_3 crystals of different crystallographic habits. Tatibouet *et al.* (*22*) studied the oxidation of butenes on unsupported MoO_3 crystallites. Hernandez and Ozkan (*23*) have studied the structural specificity of MoO_3 in C-4 hydrocarbon oxidation to maleic anhydride using MoO_3 samples exposing different relative amounts of side and basal plane area in steady-state reaction experiments. They used 1-butene as a starting feed material, and also investigated the oxidation of the intermediates 1,3-butadiene and furan, as well as the oxidation of maleic anhydride itself. They found that the catalyst with a higher percentage of the (010) plane exposed appeared to promote complete oxidation for all feed materials, whereas the sample with a lower percentage of basal plane catalyzed selective oxidation more readily. Using Raman spectroscopy in conjunction with the reaction studies, they were able to relate differences in selectivity for maleic anhydride to the presence of different Mo–O sites on the crystal planes of MoO_3. Spectra indicated that the basal (010) planes may contain relatively more Mo–O–Mo sites, while the side (100) planes had relatively more Mo=O sites exposed.

Ozkan *et al.* (*24*) have also used *in situ* Raman spectroscopy with isotopic labeling technique to investigate the oxygen inser-

tion pathway in C-4 hydrocarbon oxidation to maleic anhydride over MoO_3 catalysts. By first reducing the MoO_3 with hydrocarbon, and then reoxidizing with $^{18}O_2$, they were able to observe shifts in the Raman spectra due to the incorporation of $^{18}O_2$ into the catalyst. Results obtained through this technique further supported their proposal that Mo=O was the site responsible for selective oxidation, while total oxidation products were formed more readily over bridging Mo–O–Mo sites.

Until recently, the study of the structural effects of MoO_3 had not been extended to the partial oxidation of methane to formaldehyde. Vorob'eva *et al.* (*25*), however, reported on the oxidation of methane over MoO_3 crystals which were subjected to shear deformation treatment. Catalysts treated in this manner were reported to give almost no complete oxidation products. This work was expanded to test the mechanical activation of Mo-, V-, W-, and Fe-containing systems for methane oxidation (*26*). Such reports indicate that modification of the crystal habit of MoO_3 by other methods, such as thermal treatment, may also show effects of structural differences.

The studies presented here are the results of our investigation into the structural specificity of unsupported MoO_3 for the partial oxidation of CH_4. The oxidation of HCHO, CH_3OH, and CO was also studied to examine the reaction scheme of oxidation over these catalysts. MoO_3 samples were prepared by temperature-programmed techniques to preferentially expose different crystal planes. In order to relate structure to activity and selectivity, careful characterization was performed on the catalyst samples. Characterization included X-ray diffraction, laser Raman spectroscopy, *in situ* laser Raman spectroscopy with isotopic labeling, scanning electron microscopy with three-dimensional imaging, X-ray photoelectron spectroscopy, BET surface area measurement, and temperature-programmed reduction (TPR). Results from these characterization studies were used in conjunction with catalytic activity and selectivity experiments to investigate the reaction pathway of the partial oxidation of methane to formaldehyde over MoO_3 catalysts.

EXPERIMENTAL METHODS

Catalyst Preparation

Thermal treatment techniques were used to prepare four different MoO_3 samples of different basal (010) to side (100) plane ratios. The first, denoted MoO_3-C, was prepared by a technique based on that reported by Hernandez and Ozkan (*23*). MoO_3 (Aldrich Chemical Co.) was calcined under an O_2 stream using a temperature programmable furnace (Lindberg 54000). The MoO_3 was heated to 675°C at a rate of 20°C/min, then held at 675°C for 1 h. This technique produced rather thick MoO_3 crystals.

The second technique used to prepare MoO_3 samples preferentially exposing different crystal planes, also based on Hernandez and Ozkan (*23*), was to melt MoO_3 samples by heating them to 795°C, and holding them at that temperature for 12 min. Upon rapid cooling, long, thin crystallites were formed. These samples will be referred to as MoO_3-R.

While the third and fourth samples were not used in reaction runs, they provided valuable information about the structure of MoO_3. The third sample, denoted MoO_3-V, was formed by vapor deposition of MoO_3. These crystals were very thin, with almost no visible side plane. The fourth sample, denoted MoO_3-M, was prepared by oxidizing a thin (25-μm) sheet of Mo metal at 610°C for 12 h, following the procedure outlined by Abon *et al.* (*19*). This method yielded a sample composed of crystals of uniform size and shape with visible side planes exposed.

The differences between these samples of MoO_3 are shown in the scanning electron micrographs of Fig. 1.

Catalyst Characterization

BET surface area measurement. The surface areas of the catalyst samples were mea-

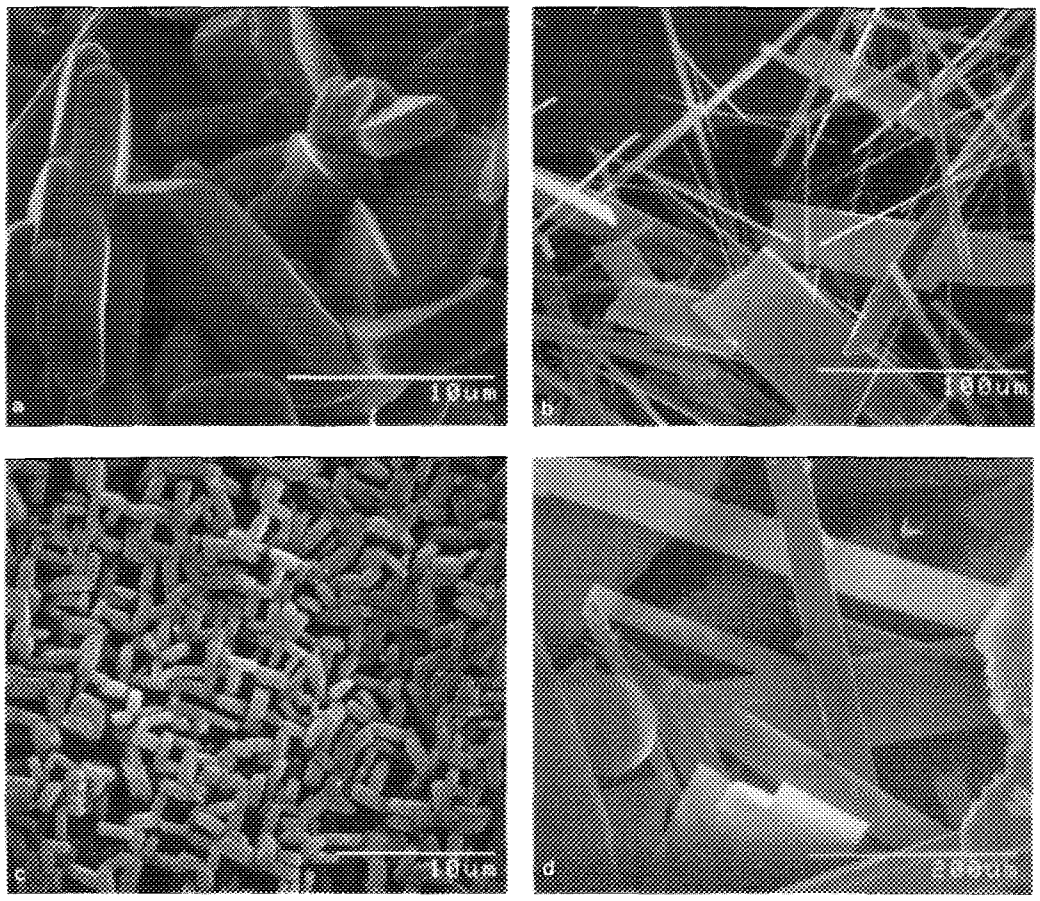

FIG. 1. Scanning electron micrographs of MoO_3 samples: (a) MoO_3-C, (b) MoO_3-R, (c) MoO_3-M, and (d) MoO_3-V.

sured by the BET method, using a Micromeritics Accusorb 2100E, with Kr as the adsorbate.

X-ray diffraction. Diffraction patterns for each sample were obtained using a Scintag PAD-V Diffractometer with Cu K_α radiation (1.543 Å), operated at 45 kV and 20 mA.

Laser Raman spectroscopy. Raman spectra of the samples were obtained using either a Spex Triplemate Raman spectrometer with CCD detector or a Spex Double Monochromator Model 1403. The 514.5 nm line of a 5-W argon iron laser (Spectra Physics) was used as the excitation source. Most spectra were accumulated at 10 mW of laser power.

X-ray photoelectron spectroscopy. XPS spectra were obtained using a Physical Electronic/Perkin–Elmer Model 550 ESCA/Auger spectrometer at 15 kV, 20 mA. The X-ray source was Mg K_α radiation (1253.6 eV). The C 1*s* binding energy (284.6 eV) was used as a reference.

Scanning electron microscopy. Micrographs were taken to study the topography of the catalyst samples, as well as to determine the basal-to-side plane ratios of each sample. The micrographs were obtained using a Hitachi S-510 scanning electron microscope, with an acceleration voltage of 25 kV. Stereo pairs of MoO_3 crystals were obtained by dispersing a sample of the MoO_3

on a carbon disk. This was done by adding the sample to a small amount of acetone and placing a drop of the suspension on the carbon disk. This method allowed crystals of MoO_3 to be isolated. Following the method used by Hernandez and Ozkan (*23*), a micrograph of the crystal was taken, and then the sample stage of the microscope was tilted by 10° and another micrograph was taken of the same crystal. These stereo pairs were then digitized using an Eikonix 78/99 digitizer and Dipix Aries-III software. Digitization of these pairs allowed the images to be used in conjunction with a computer program (*27*) run on a VAX 8550 computer, which enabled the identification of crystal planes. The area of the identified planes was then quantified by the program with an accuracy which would not be possible with two-dimensional images. The accuracy of the computer program was tested with a cubic crystal, NaCl. The area calculated for three different crystal planes of the NaCl crystal was found to be within 2–7% of each other.

Reaction Studies

Reactor system. Steady-state reaction studies were performed using the system shown in Fig. 2. The composition and the flow rate of the feed stream were controlled using a set of Tylan mass flow controllers calibrated for each specific gas used (CH_4,N_2, O_2). Introduction of HCHO into the feed stream was accomplished through the use of a sealed stainless steel beaker with heated inlet and outlet tubes. Paraformaldehyde powder (J. T. Baker Inc.) was placed in the beaker which was held at 70°C. An oxygen/nitrogen stream was passed through the beaker, and the desired HCHO concentrations were achieved by controlling the flow rate of the stream through the beaker. Methanol was introduced into the feed using a syringe pump (Sage) which allowed a steady amount of CH_3OH to be injected into the gas stream. CO was introduced by recalibrating the methane mass flow controller to control the flow of CO. A union tee was inserted in the feed line prior to the entrance of the reactor. A metering valve (Whitey) was inserted on one arm of the tee so that the flow rate of the feed gases could be adjusted to obtain any desired total flow rate through the reactor.

The reactor used was a quartz fixed-bed reactor with an inner diameter of 5 mm at the catalyst bed portion. A quartz frit was used to hold the catalyst bed in place. The exit diameter was decreased to 2 mm i.d. to allow the gas stream to rapidly leave the heated catalyst bed. The catalyst bed was heated using resistive heating cartridges and a stainless steel block. The reactor was connected to the feed flow system by means of Ultra-torr brand fittings and a four-port valve (Valco), which allowed the feed stream to bypass the reactor so feed analysis could be performed. All lines of the feed and reaction system were heated to prevent condensation in the lines.

An automated on-line gas chromatograph (Hewlett–Packard 5890 Series II) was used in conjunction with two HP 3386A integrators for feed and product analyses. The gas chromatograph had both a flame ionization detector (FID) and a thermal conductivity detector (TCD). A 5-ft Hayesep T column was used with both detectors for separation of CO_2, CH_3OH, HCHO, and other partial oxygenates. A molecular sieve 5A column (10 ft) was used in conjunction with a four-port valve on the TCD to separate CH_4, N_2, O_2, and CO. N_2 was included in the feed stream as an internal calibration for GC analysis. Reactor effluent could also be directed to a GC/Mass Spectrometer (Hewlett-Packard MS Engine 5989A) for further analysis.

Reaction parameters. Reaction experiments were designed to enable comparison of selectivities at equal methane conversion levels, as well as comparison of reaction rates at equal residence time. Equal residence time was based on equal total surface area and equal total flow rate of feed gases. The bed volume was also kept constant by diluting the catalyst. All reaction experiments were performed at 650°C and at atmospheric pressure. For methane oxidation

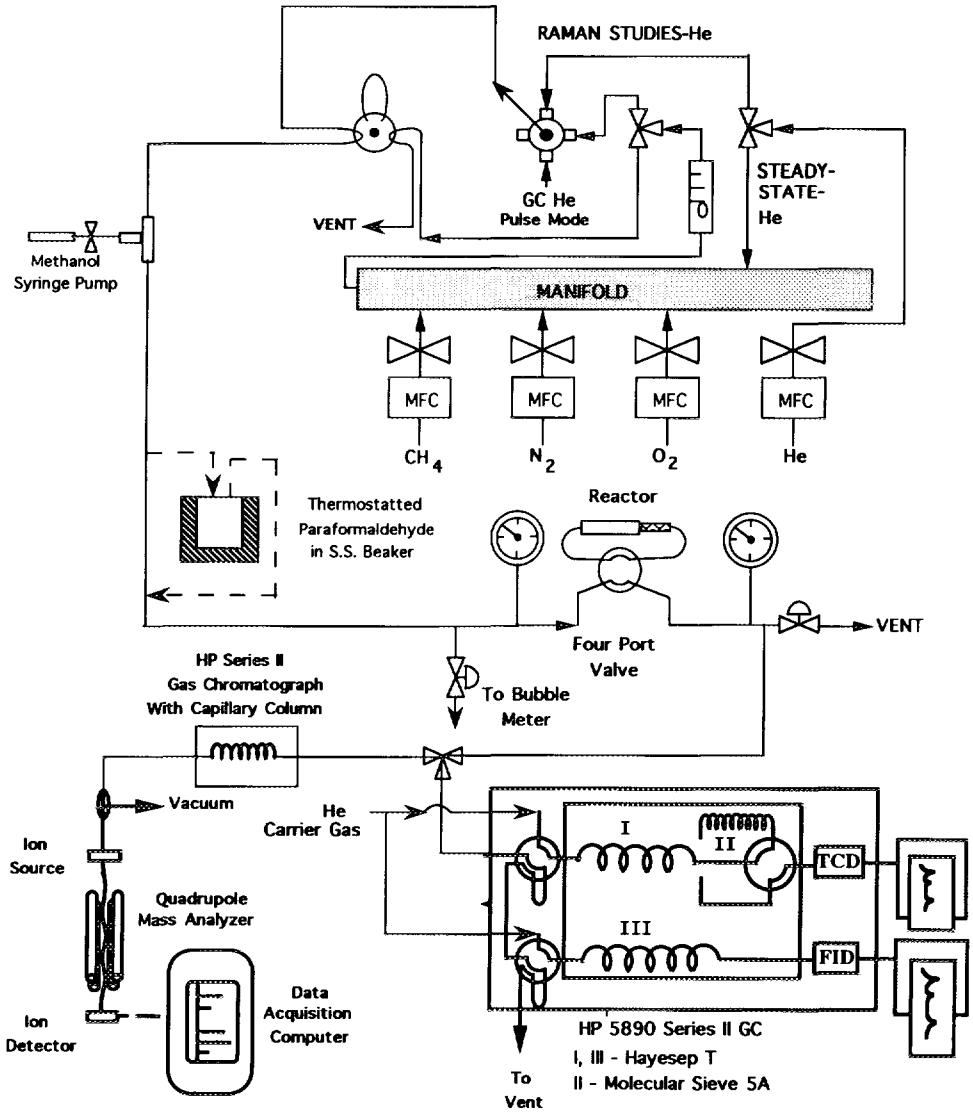

FIG. 2. Reaction system used for steady-state oxidation experiments.

runs, the $CH_4 : O_2$ ratio was varied from 2.97 to 17.22. The methane concentration was held at 67.0 vol% for all runs, and O_2 and N_2 concentrations were changed to achieve the desired CH_4/O_2 ratio.

Formaldehyde and CO oxidations were performed at two different feed concentrations. For formaldehyde oxidation, the feed concentrations were 5.5% HCHO–10.9% O_2 and 12.0% HCHO–2.2% O_2. CO oxidation was performed at feed concentrations of 3.2% CO–10.3% O_2 and 9.8% CO–2.1% O_2.

Blank reactor experiments were also performed for all feed conditions listed above.

Temperature-Programmed Reduction Studies (TPR)

Temperature-programmed reduction was performed using a system consisting of a feed manifold, a reaction chamber, and a thermal

conductivity detector. A vacuum system used in conjunction with the TPR apparatus allowed for an ultimate vacuum of 10^{-7} Torr for degassing samples prior to reduction. A quartz U-tube was used for the sample chamber, and an IBM-compatible computer was used for instrument control and data acquisition. The system is described in detail elsewhere (*28*). The sample size used for the experiments was 53 mg, except when comparison between MoO_3-C and MoO_3-R was based on equal surface area rather than equal weight. The heating rate was 5°C/min with a reducing mixture composed of 6% H_2 in N_2.

In situ Laser Raman Spectroscopy with Isotopic Labeling Technique

In situ laser Raman spectroscopy experiments were performed using a specially designed *in situ* cell and cell holder which have been described in detail previously (*24*). The catalyst was placed in the quartz cell which was aligned using the cell holder in the sample compartment of the Triplemate spectrometer. The cell and holder were heated and a base spectrum was recorded. The sample was then reduced at 450°C under a flow of 6% H_2 in N_2 at 60 cm^3 (STP)/min total molar flow rate for 1 h. This allowed for a "partial" or surface reduction of the catalyst sample, rather than a bulk reduction, as evidenced by TPR experiments performed under similar conditions. The cell was flushed with He for 10 min and isolated from the flow system. A spectrum was taken of the reduced sample at 450°C, and the cell was pressurized using a mixture of 25% $^{18}O_2$ in N_2 and allowed to sit for 30 min at 450°C. During this time, spectra were accumulated at regular intervals using the CCD (Couple Charged Device) detector. After 30 min, fresh isotopic mixture was allowed to enter the cell, and the cycle was repeated until there was no further increase in intensity of the spectrum.

RESULTS

Catalyst Characterization

X-ray diffraction. When the X-ray diffraction patterns obtained for the four MoO_3 samples were compared with the patterns in the literature (*29*), the *d*-spacings were found to closely match the literature values. However, the relative intensities of the peaks varied with the MoO_3 preparation. Most noticeably, the intensities associated with planes (0*k*0) are larger in the MoO_3-R and especially in the MoO_3-V samples. This trend is shown in Table 1, which tabulates the ratio of the sum of the intensities of *d*-spacings attributed to side planes (*h*00) to the sum of the intensities of *d*-spacings attributed to basal planes (0*k*0) for each MoO_3 sample. The unit cell dimensions for the orthorhombic system are chosen as a = 3.9639 Å, b = 13.856 Å, and c = 3.6996 Å.

TABLE 1

Ratio of X-Ray Diffraction Intensities for Side to Basal Plane of MoO_3

Sample	$\Sigma I_{h00}/\Sigma I_{0k0}$
MoO_3-M	0.080
MoO_3-C	0.062
MoO_3-R	$\leq$0.001
MoO_3-V	~0

Laser Raman spectroscopy. Raman spectra for all four samples are shown in Fig. 3. The major bands were located at 111, 124, 153, 193, 231, 278, 287, 333, 371, 665, 818, and 995 cm^{-1}, and agree with those previously reported in the literature (*30*). While the actual band positions did not change among the samples, the relative intensities did change, the most noticeable being those associated with the 818-cm^{-1} and 995-cm^{-1} bands. The band at 818 cm^{-1} has been assigned to the stretching vibrations of the bridging oxygen bonds (Mo–O–Mo) and the band at 995 cm^{-1} to Mo=O stretching vibrations (*30*). A similar trend was observed when the intensities of the 193-cm^{-1} and 231-cm^{-1} bands, which are due to Mo–O–Mo deformations, were compared with those of 278-cm^{-1} and 371-cm^{-1} bands, which are associated with the Mo=O defor-

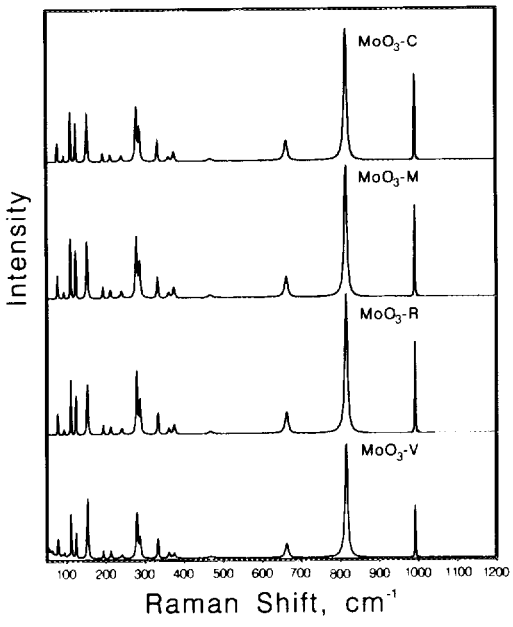

FIG. 3. Raman spectra of MoO_3 samples.

mations. The band at 665 cm^{-1}, which has been attributed to the OMo_3 vibrations (*30*), has also decreased in intensity with respect to the 818-cm^{-1} band in the spectrum of MoO_3-V. These trends are summarized in Table 2.

X-ray photoelectron spectroscopy. The binding energy values obtained for Mo $3d_{5/2}$, Mo $3d_{3/2}$ and O 1*s* are shown in Table 3. Comparison to literature values (*3*) shows that the binding energy values agree with the expected values quite closely. However, MoO_3-M has shown an asymmetrical peak for the O 1*s* binding energy. This peak could

TABLE 2

Ratio of Raman Band Intensities for (Mo=O)/(Mo-O-Mo) Vibrations

Sample	I_{995} cm^{-1}/I_{818} cm^{-1}
MoO_3-M	0.71
MoO_3-C	0.66
MoO_3-R	0.62
MoO_3-V	0.47

TABLE 3

Binding Energy Values for MoO_3 Samples

Sample	Binding energy (eV)		
	Mo		O
	$3d_{5/2}$	$3d_{3/2}$	1 *s*
MoO_3-M	232.82	235.97	530.87, 533.22
MoO_3-C	232.948	236.13	530.90
MoO_3-R	232.79	235.95	530.77
MoO_3-V	233.05	236.21	531.03

be resolved using a computer program to deconvolute the asymmetrical peak into the two values at 530.87 and 533.22 eV.

Scanning electron microscopy and three-dimensional imaging. The micrographs shown in Figure 1 reveal some important differences in the MoO_3 samples. MoO_3-C crystals have an average length of about 13 μm, while MoO_3-R is composed of long, lathe-like crystals, on the order of 100–200 μm. The crystals of MoO_3-M, while exposing side plane area, are much smaller than those of MoO_3-C, on the order of 3–5 μm. Crystals of MoO_3-V are the largest of all, on the order of 500 μm. Stereo pairs of MoO_3-C and MoO_3-R were used for basal (010) to side (100) plane area quantification for these two samples. An example of a stereo pair is shown in Fig. 4 for the MoO_3-C sample. The basal to side plane area ratios were found to be 3.5 for MoO_3-C and 6.5 for MoO_3-R, showing MoO_3-R having almost two times as much relative basal plane area as MoO_3-C. The surface area measurements also reflect the differences in crystal size of these samples, with MoO_3-C having a surface area of 0.32 m^2/g and MoO_3-R of 0.12 m2/g.

Reaction Studies

Steady-state oxidation of methane. The first set of reaction studies compared product selectivities obtained over MoO_3-C and MoO_3-R in methane oxidation. All reaction data were obtained at steady-state, which

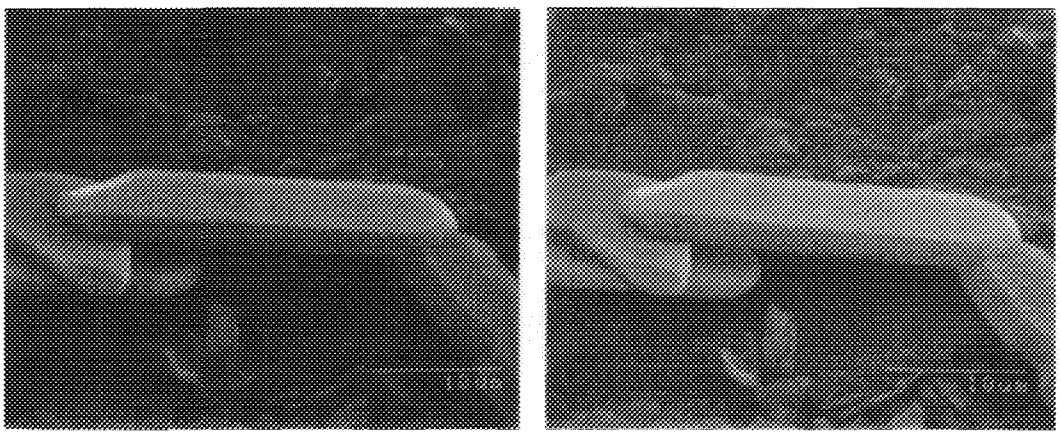

FIG. 4. Stereo pairs of scanning electron micrographs for MoO_3-C.

was reached after 4 h as evidenced by the constant conversion and product distributions. Several reaction runs were continued for periods of 18–20 h with no significant changes in the conversion or product distribution. Figure 5a shows a comparison of selectivities to HCHO, CO_2, and CO at an equal methane conversion level of 2% over the two catalysts at CH_4/O_2 ratio of 3.55. The most striking difference between the two MoO_3 preparations was that MoO_3-C was seen to be about twice as selective for the partial oxidation product of interest, HCHO, than was MoO_3-R, while MoO_3-R was, likewise, about twice as selective for CO_2 as was MoO_3-C. Also, CO was produced in quantifiable amounts only over MoO_3-R. These same trends were observed when selectivities were compared using a CH_4/O_2 ratio of 5.56, this time keeping the methane conversion level constant at 1% (Fig. 5b).

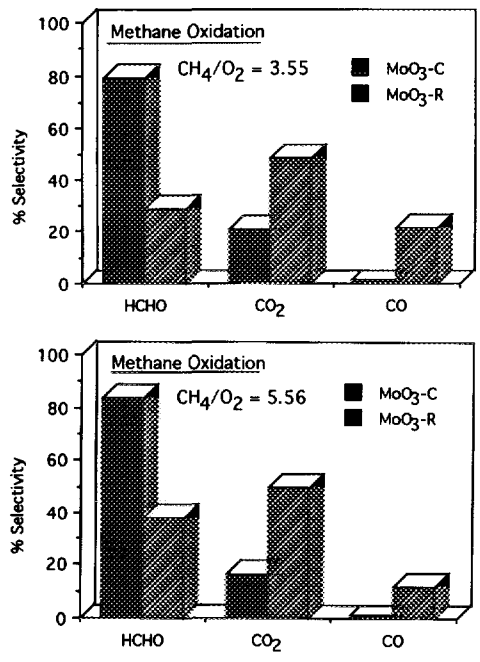

FIG. 5. Comparison of selectivities over MoO_3-C and MoO_3-R at equal conversion levels in methane oxidation.

Figure 6 shows the variation in production rates of HCHO, CO, and CO_2 at two different CH_4/O_2 feed ratios using equal residence time, when methane conversion levels for the two catalysts were not necessarily equal. It is seen that the trend for MoO_3-C to produce more HCHO than does MoO_3-R continues with change in feed ratios. It is interesting to note that when the CH_4/O_2 feed ratio was decreased, there was a slight decrease in HCHO formation rate, accompanied by a slight increase in CO_x formation rate with the increase in CO formation rate over MoO_3-R being more noticeable.

The ratio of HCHO yield to CO_x yield is plotted in Fig. 7 as a function of oxygen

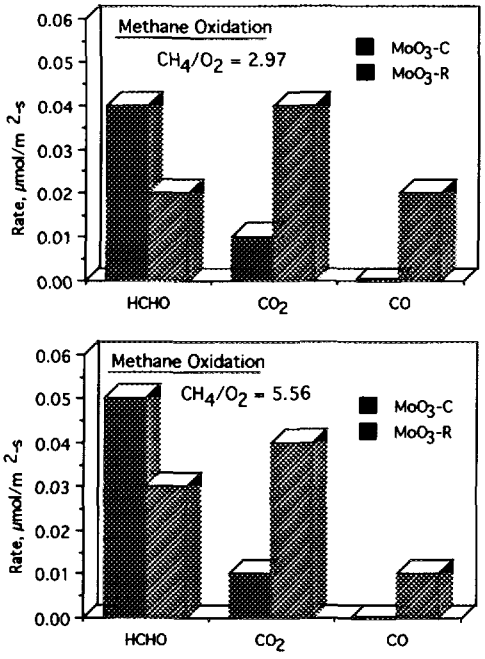

FIG. 6. Comparison of production rates over MoO_3-C and MoO_3-R at different CH_4/O_2 ratios in methane oxidation.

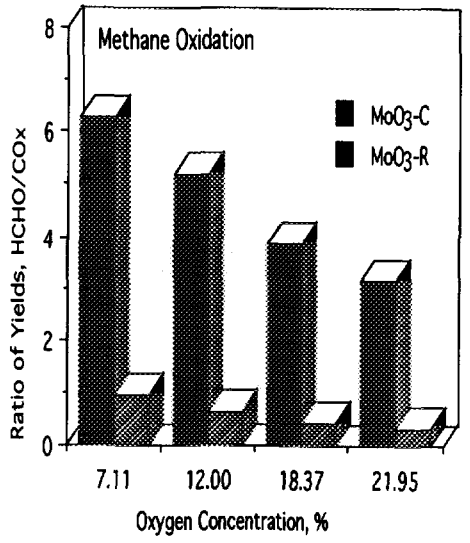

FIG. 7. Variation of ratio of HCHO to COx yield with oxygen concentration in methane oxidation.

concentration. The percentage of methane in the feed was held constant. This ratio decreased over both catalysts as the oxygen concentration in the feed increased. Also, the yield ratio of HCHO/CO_x was much greater over the MoO_3-C sample than over the MoO_3-R sample at every oxygen concentration tested.

No quantifiable conversion of methane was observed during the blank reactor experiments.

Steady-state oxidation of formaldehyde. The second set of experiments involved using formaldehyde itself as a feed material in order to gain insight into the reaction scheme. The conversion and production rates over the two catalysts are compared at two different feed compositions in Fig. 8. Under both feed conditions, MoO_3-R was seen to be more active than MoO_3-C in formaldehyde conversion. The more striking difference between the two catalysts, however, was seen in product distribution. For both feed compositions, the ratio of CO_2 rate to CO rate was greater over MoO_3-R than it was over MoO_3-C. For the run where the HCHO concentration was 5.5%, the CO_2/CO rate was 0.146 over MoO_3-C and

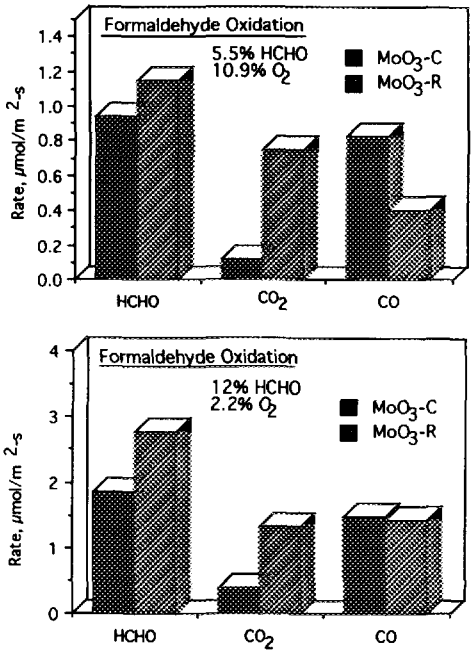

FIG. 8. Rates of conversion and production at different feed compositions in formaldehyde oxidation.

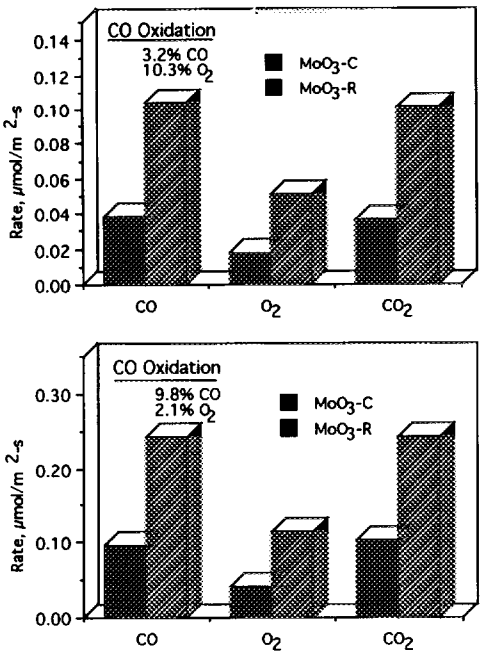

FIG. 9. Rates of conversion and production at different feed compositions in CO oxidation.

1.88 over MoO_3-R. For the run where the HCHO concentration was 12%, this ratio was 0.257 and 0.917 for MoO_3-C and MoO_3-R, respectively.

Another interesting observation is that using feed compositions representing oxygen-rich conditions, CO_2 yield was seen to be twice as high as the CO yield over MoO_3-R. When the feed composition was representative of oxygen lean conditions, the same catalyst yielded slightly more CO than CO_2, indicating that there may be multiple pathways leading to the production of CO_2 and CO from HCHO over MoO_3 catalysts. Over MoO_3-C, CO was the major product for both feed compositions.

Blank reactor experiments performed using the same feed conditions showed the main oxidation product of HCHO to be CO.

Steady-state oxidation of carbon monoxide. CO oxidation rates were also compared at two different feed compositions over both catalyst preparations, and the results are presented in Fig. 9. As was found in the case of other feed materials, MoO_3-R was more active in production of CO_2 than MoO_3-C. Blank reactor runs showed no quantifiable conversion of CO.

Temperature-Programmed Reduction Studies

The TPR profiles obtained over both catalysts are shown in Fig. 10. One important difference between the two profiles was found in the shoulder-like peak that appeared around 550°C. Over MoO_3-R, this shoulder-like peak was slightly more pronounced, and the slope of the shoulder was greater in MoO_3-R than in MoO_3-C, indicating that MoO_3-R was using H_2 more readily than MoO_3-C at this point in the reduction. By stopping the reduction after each peak and using XRD and the H_2 consumption, the reduction intermediates were identified. After the "shoulder-like" peak that occurs at 627°C, the closest identification of the compound appeared to be a mixture of MoO_3 and $MoO_{2.8}$. After the temperature maximum at 767°C, the compound was identified as Mo_4O_{11}. After the 840°C maximum, the sample was found to have been reduced

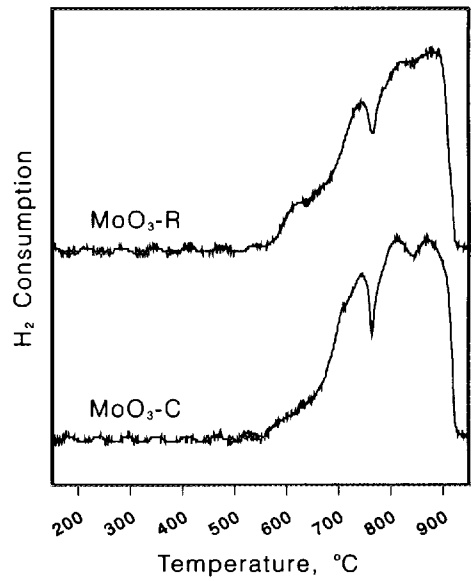

FIG. 10. H_2 TPR profiles of MoO_3 samples.

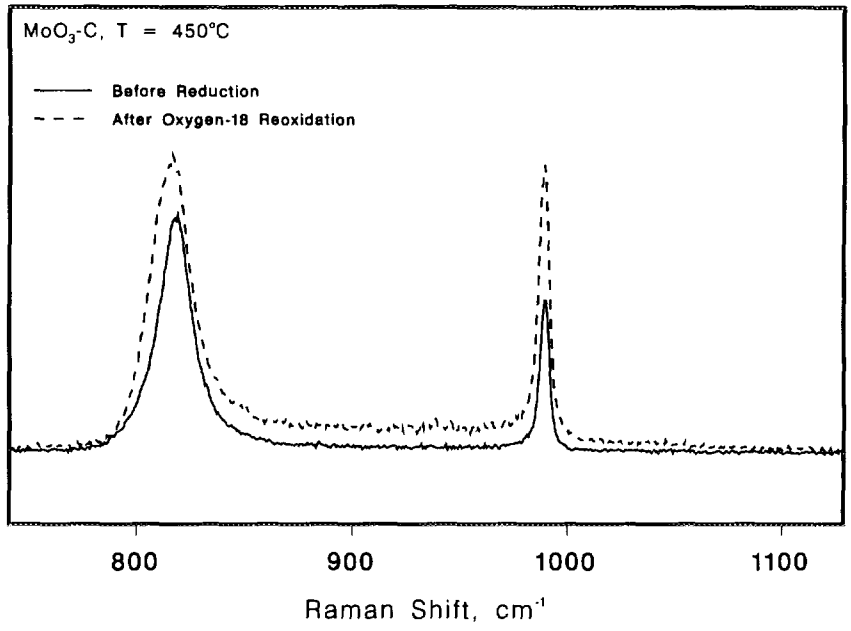

FIG. 11. Raman spectra before reduction and after reoxidation with $^{18}O_2$.

to MoO_2, and after 920°C peak, the sample was found to be a mixture of MoO_2 and Mo metal.

In situ Laser Raman Spectroscopy with Isotopic Labeling Technique

The Raman spectra of the high wavenumber region (750–1150 cm^{-1}) is shown in Fig. 11 both before partial reduction and after reduction followed by reoxidation with $^{18}O_2$. Several interesting observations are apparent. First, the band at 818 cm^{-1} (Mo–O–Mo) has shifted slightly and broadened, with the FWHM increasing by 33% after the reoxidation with $^{18}O_2$, while the band at 995 cm^{-1} (Mo=O) does not appear to have broadened much or shifted. The second observation is that before reduction, the 818 cm^{-1} band was the major band in the region, while after reoxidation, the intensities of the bands at 818 and 995 cm^{-1} were approximately equal, indicating that Mo=O sites have been more fully reoxidized than Mo–O–Mo sites. The 665 cm^{-1} band did not show any noticeable shift after reoxidation, only a slight broadening. The relative intensity of the band did not show an increase after reoxidation.

DISCUSSION

Our steady-state reaction studies of partial oxidation of methane over molybdenum trioxide catalysts preferentially exposing different crystal planes provided important insight into the reaction scheme that leads to the formation of formaldehyde and carbon oxides from methane. Especially when combined with characterization results, these studies also provided important clues as to the nature of active sites involved in the various catalytic steps of the reaction network.

Molybdenum trioxide samples prepared by using different thermal treatment techniques led to significant differences in crystal size and dimensions, exposing different crystal planes preferentially. While scanning electron microscopy images provided visual evidence of the changing crystal dimensions, the three-dimensional imaging

technique allowed us to quantify the surface area exposed by different crystal planes with an accuracy that would not be possible with two-dimensional images. X-ray diffraction patterns further verified the preferred exposure of different crystal planes suggested by scanning electron microscopy, by showing significant differences in relative intensities associated with diffractions from (0k0) and (h00) planes.

Laser Raman spectroscopy studies, on the other hand, not only revealed significant differences in the relative band intensities of MoO_3 samples exposing different ratios of (010) to (100) planes, but also provided important clues about the nature and relative abundance of the oxygen sites in these crystal planes. The most striking difference was the relative intensity of the 818-cm^{-1} band to the 995-cm^{-1} band. The intensity of the 818-cm^{-1} band which is associated with the stretching vibration of Mo–O–Mo sites consistently increased relative to the 995-cm^{-1} band which is due to the stretching vibration of the Mo=O terminal sites with increased exposure of the (010) plane area. A similar trend was observed when the intensities of the 193-cm^{-1} and 231-cm^{-1} bands, which are due to Mo–O–Mo deformations, were compared with those of the 278-cm^{-1} and 371-cm^{-1} bands, which are associated with the Mo=O deformations. Also, the band at 665 cm^{-1}, which is associated with the OMo_3 vibrations, became noticeably weaker in the spectra accumulated from the MoO_3-V sample, which exposed very little (100) plane.

Another interesting point derived from the characterization experiments was the X-ray photoelectron spectroscopy results which showed the O 1s peak to be deconvoluted into two peaks for the sample which had the largest percentage of the (100) plane. The presence of a second O 1s peak has been attributed to OH groups bound on the surfaces of transition metal oxides (*31*). If this assumption is correct, our results may be suggesting the presence of OH groups on the side planes in the presence of water at ambient conditions.

Reaction results of methane oxidation have shown significant differences in product distribution obtained over the basal and side planes of MoO_3 crystals. The catalysts which preferentially exposed the (010) plane produced more complete oxidation products than the catalysts which exposed a relatively larger side plane area. This trend was seen to be true at every oxygen concentration and conversion level used in this study. The selectivity for HCHO and CO_x was seen to be affected by the concentration of gas phase oxygen in the feed. As the oxygen concentration was increased, the selectivity for HCHO dropped as the selectivity for CO_x rose, indicating that the gas-phase oxygen could be playing a role in the further oxidation of HCHO. The presence of catalytic anisotropy was also evident when reaction intermediates such as HCHO, CO, CH_3OH were used as feed material. The complete oxidation of the partial oxygenates was also seen to be more heavily favored over catalysts that exposed the (010) planes preferentially.

Oxidation experiments using HCHO as the feed showed mainly CO as the product when no catalyst was present in the reactor, indicating that the further oxidation of HCHO may occur in the gas phase. However, when catalyst was present, MoO_3-R was the more active of the two catalysts, and the ratio of CO_2/CO was greater over MoO_3-R than over MoO_3-C. Thus it appears that several pathways may be contributing to the further oxidation of HCHO including homogeneous oxidation of HCHO, direct catalytic oxidation of HCHO to CO_2 and catalytic oxidation of HCHO to CO_2 through an intermediate step of CO formation.

CO oxidation experiments showed that the contribution of gas phase oxidation of CO to CO_2 was minimal, as the blank reactor showed no quantifiable conversion. Also, these studies showed a higher yield of complete oxidation products over catalysts exposing relatively larger basal surface area, suggesting a more direct involvement of

TABLE 4

H_2 Consumption Ratios

Temperature range (°C)	mol H_2 Consumed/m^2(MoO_3-C) / mol H_2 Consumed/m^2(MoO_3-R)
540–570	0.380
570–600	0.264
600–630	0.236
630–660	0.283
660–690	0.402
690–720	0.422

Mo–O–Mo sites in the oxidation of CO to CO_2.

As traces of methanol appeared in our chromatograms, methanol oxidation was also performed over these catalysts at 650°C, in order to assess the feasibility of methanol as a reaction intermediate in HCHO formation. The most interesting result of these studies was that, at the reaction temperature of 650°C, complete conversion of methanol was reached, indicating that most of the methanol which may have been produced via an oxidation of CH_4 would have been converted to HCHO or CO_x.

Temperature programmed reduction studies provided information about the relative reducibility of different oxygen sites on MoO_3 surfaces. TPR profiles show that MoO_3-R is more easily reduced during the first reduction step than is MoO_3-C. As there are relatively more Mo–O–Mo sites exposed on the MoO_3-R sample than on the MoO_3-C sample, this suggests that the Mo–O–Mo sites are more easily reduced than the Mo=O sites. This is also seen by comparing the ratio of H_2 consumed over MoO_3-C to H_2 consumed over MoO_3-R, as is shown in Table 4. The same trend was verified when experiments were repeated keeping the surface area constant in the TPR sample chamber.

In situ Raman spectroscopy provided further clues about oxidation sites as well as the regeneration process for the reduced sites. In one set of experiments, catalysts were reduced with care taken to limit the reduction primarily to the surface using the TPR patterns as guidelines to define time, temperature and hydrogen concentration in the reduction step. When the sample was reoxidized with labeled oxygen ($^{18}O_2$), the Mo–O–Mo sites showed a substantial amount of gas phase oxygen incorporation, as evidenced by the band broadening of the 818 cm^{-1} band in Fig. 11. The Mo=O sites, however, do not seem to be reoxidized as readily with gas phase oxygen, as there is not a noticeable band broadening in the 995-cm^{-1} band although its intensity returns to the same level that it was prior to reduction. This indicates that perhaps reoxidation is not only occurring through the gas phase oxygen ($^{18}O_2$, in this case), but more readily by bulk diffusion of oxygen through the catalyst lattice. It is difficult to draw a conclusion about the role of OMo_3 sites, as the 665-cm^{-1} band associated with these sites does not show any indication of a major replenishment by the gas phase oxygen or a rapid diffusion from the catalyst lattice. Although it is quite possible that the replenishment of the reduced sites by bulk diffusion of lattice oxygen could be playing a role in the reoxidation of Mo–O–Mo sites, OMo_3 sites, and Mo=O sites, we suspect that this process is more prominent for the terminal oxygen (Mo=O) sites. The change in relative intensities of the 818-cm^{-1} and 995-cm^{-1} bands prior to reduction and after reoxidation seems to support this possibility. The diffusion of oxygen through the lattice has been also demonstrated in a second set of experiments where MoO_3 samples were reduced at 450°C, then flushed with He. After letting the catalyst samples remain in a He atmosphere for 12 h, the intensity loss in the spectrum caused by reduction was recovered although no gas phase oxygen was brought into contact with the catalyst surface.

The data gathered in these studies suggest a reaction pathway for the partial oxidation of CH_4 to HCHO in which the oxygen insertion to form HCHO is thought to be taking

TABLE 5

Rate Based on Side Plane (100) Area (molecules $HCHO/m^2$ side plane-s)

Catalyst	67% CH_4, 22% O_2	67% CH_4, 12% O_2
MoO_3-C	1.0×10^{17}	1.3×10^{17}
MoO_3-R	1.0×10^{17}	1.5×10^{17}

place over the Mo=O sites located on the side planes, accounting for the increased selectivity to HCHO over the catalyst containing relatively more of these sites. When the rates of formation of HCHO are normalized with respect to (100) plane surface area, the rates over the catalysts with different side to basal plane area ratios appear to be equal or very close to each other, as shown in Table 5. This evidence provides further support for the possibility that the Mo=O sites located on the (100) planes are responsible for the formation of HCHO. Chung *et al.* (*32*), who have investigated structural specificity of MoO_3 in methanol oxidation, have proposed a similar role for the Mo=O sites. They found HCHO and CO being produced from methoxy groups mainly on the terminal Mo=O site, while the bridging oxygen sites were responsible for high-order products such as dimethyl ether. At high temperatures, they found that shear planes appear, promoting diffusion of bulk oxygen to the surface.

The nonselective oxidation of CH_4 appears to take place through a complex network of multiple steps which can proceed in parallel or in series. However, the results obtained in this study seem to indicate that Mo–O–Mo sites are more likely to promote complete oxidation. While the Mo–O–Mo sites appear to promote direct oxidation of CH_4 to CO and further oxidation of CO to CO_2, the formation of CO from HCHO can proceed both in the gas phase and over Mo=O sites.

The catalytic job distribution suggested by these studies also seems to be in agreement with our earlier investigation on partial oxidation of methane over SiO_2-supported molybdena catalysts where we found the Mo=O sites present on the surface at low loading levels to be more selective for HCHO and the Mo–O–Mo bridging oxygen sites, which form at the expense of terminal oxygen sites, to lead to complete oxidation (*13*).

In conclusion, the partial oxidation of methane to formaldehyde over MoO_3 catalysts has been found to be a structure-sensitive reaction. Evidence gathered from our characterization and reaction studies has allowed the formulation of a reaction scheme, and indicates that the sites responsible for production of HCHO are Mo=O, which reside preferentially on the side planes of the MoO_3 crystal, while those that promote total oxidation are the Mo–O–Mo sites, which are more abundant on the basal planes of the crystal. These conclusions are reinforced by TPR data which show that Mo–O–Mo sites are more readily reduced than are Mo=O sites, as well as by *in situ* Raman data which show the Mo–O–Mo sites to be reoxidized more readily by gas-phase oxygen, while the Mo=O sites appear to be reoxidized more readily by lattice oxygen.

Our studies using transient isotopic labeling technique under steady-state reaction conditions provided further evidence supporting the conclusions drawn in this article while helping us gain further insight into the possible oxygen insertion mechanism in partial oxidation of methane. The details of these studies will be presented in the next paper of this series (*33*).

ACKNOWLEDGMENTS

The financial support from National Science Foundation through Grant CTS-8912247 is gratefully acknowledged. The authors also thank Professor Robert S. Brodkey for his discussions on three-dimensional imaging and the use of the digitization equipment, and Professor Rodney T. Tettenhorst for his discussions on the crystallography of MoO_3. The authors also acknowledge Ms. Liping Zhang for her technical assistance in the TPR experiments.

REFERENCES

1. Fox, J. M., Cheng, T. P., and Degen, B. D., *Chem. Eng. Prog.* **86**,(4), 42 (1990).

2. Pitchai, R., and Klier, K., *Catal. Rev.-Sci. Eng.* **28**(1), 13 (1986).
3. Foster, N. R., *Appl. Catal.* **19,** 1 (1985).
4. Brown, M. J., and Parkyns, N. D., *Catal. Today* **8,** 305 (1991).
5. Solymosi, F., Tombacz, I., and Kutsan, G., *J. Chem. Soc. Chem. Commun.*, 1455 (1985).
6. Otsuka, T., Komatsu, T., Jinno, Y., Uragami, Y., and Morikawa, A., *in* "Proceedings, 9th International Congress on Catalysis, Calgary, 1988" (M. J. Phillips and M. Ternan, Eds.), p. 915. Chem. Institute of Canada, Ottawa, 1988.
7. Liu, H. F., Liu R. S., Liew, D. Y., Johnson, R. E., and Lunsford, J. H., *J. Am. Chem. Soc.* **106,** 4117 (1984).
8. Khan, M. M., and Somorjai, G. A., *J. Catal.* **91,** 263 (1985).
9. Barbaux, Y., Elamrani, A., and Bonnelle, J. P., *Catal. Today* **1,** 147 (1987).
10. Spencer, N. D., and Pereira, C. J., *AIChE J.* **33**(11), 1808 (1987).
11. Spencer, N. D., *J. Catal.* **109,** 187 (1988).
12. Spencer, N. D., Pereira, C. J., and Grasselli, R. K., *J. Catal.* **126,** 546 (1990).
13. Smith, M. R., and Ozkan, U. S., *Catalysis Letters*, in press.
14. Kasztelan, S., Payen, E., and Moffat, J. B., *J. Catal.* **112,** 320 (1988).
15. Volta, J. C., Desquesnes, W., Moraweck, B., and Coudurier, G., *React. Kinet Catal. Lett.* **12**(3), 241 (1979).
16. Volta, J. C., Desquesnes, W., and Moraweck, B., *in* "Proceedings, 7th International Congress on Catalysis, Tokyo, 1980" (T. Seiyama and K. Tanabe, Eds.), p. 1398. Elsevier, Amsterdam, 1981.
17. Volta, J. C., Desquesnes, W., and Moraweck, B., and Coudurier, G., *in* "Proceedings, 8th International Congress on Catalysis, Berlin, 1984" Dechem, Frankfurt-am-Main, 1984.
18. Volta, J. C., and Tatibouet, J. M., *J. Catal.* **93,** 467 (1985).
19. Abon, M., Mingot, B., Massardier, J., and Volta, J. C., *in* "New Developments in Selective Oxidation" (G. Centi, F. Trifiro, Eds.). Elsevier, Amsterdam, 1990.
20. Abon, M., Massardier, J., Mingot, B., Volta, J. C., Floquet, N., and Bertrand, O., *J. Catal.* **134,** 532 (1992).
21. Bruckman, K., Haber, J., and Wiltowski, T., *J. Catal.* **106,** 188 (1987).
22. Tatibouet, J. M., Phichitkul, C., and Germain, J. E., *J. Catal.* **99,** 231 (1986).
23. Hernandez, R. A., and Ozkan, U. S., *Ind. Eng. Chem. Res.* **29**(7), 1454 (1990).
24. Ozkan, U. S., Smith, M. R., and Driscoll, S. A., *J. Catal.* **134,** 24 (1992).
25. Vorob'eva, G. A., Zhoron, V. A., Shashkin, D. P., Margolis, L. Ya., and Krylov, O. V., *Kinet. Catal.* **28,** 898 (1987).
26. Firsova, A. A., Vorob'eva, G. A., Bobyshev, A. A., Shashkin, D. P., Margolis, L. Ya., and Krylov, O. V., *Kinet. Catal.* **32,** 349 (1991).
27. Russ, K. M., Ph.D. dissertation, The Ohio State University, 1991.
28. Driscoll, S. A., Zhang, L., and Ozkan, U. S., *in* "ACS Symposium Series" (S. T. Oyama and J. W. Hightower, Eds.), in press.
29. International Centre for Diffraction Data, JCPDS, Swarthmore, PA, 1990.
30. Beattie, I. R., and Gilson, T. R., *J. Chem. Soc. A*, 2322 (1969).
31. Gasior, M., Haber, J., Machej, T., and Czeppe, T., *J. Mol. Catal.* **43** 359 (1988).
32. Chung, J. S., Miranda, R., and Bennett, C. O., *J. Catal.* **114,** 3948 (1988).
33. Smith, M. R., and Ozkan, U. S., *J. Catal.*, in press.